# The deflection angle of surface ocean currents from the wind direction

A. Bressan(*) and A. Constantin(**)

(*) Department of Mathematics, Penn State University,
University Park, PA 16802, USA.
(**) Faculty of Mathematics, University of Vienna,
Oskar-Morgenstern-Platz 1, 1090 Vienna, Austria.

e-mails: axb62@psu.edu, adrian.constantin@univie.ac.at

June 25, 2019

**Abstract**

Wind stress drives the upper ocean circulation at mid-latitudes by means of an interplay with the vertical turbulent friction and the Coriolis force, generating horizontal wind-drift currents which spiral and decay with depth. Classical Ekman theory – applied almost universally in oceanography – predicts that the angle between the vectors of the surface current and surface wind is 45°, if the coefficient of vertical turbulent mixing is constant. However, observations show that the deflection angle is usually close to 30° in arctic regions and larger than 45° in some low latitude areas, because the vertical turbulent mixing varies with depth. In contrast to Ekman's classical solution, the solutions that are available for depth-dependent eddy viscosity are quite involved and, as in data-driven studies, it is difficult to sort out spurious correlations that obscure the underlying structure. We propose a perturbative approach, providing a formula for the deviation of the deflection angle from the 45° reference value.

## 1 Introduction

As the wind blows across the ocean, it moves its near-surface waters as a result of its frictional drag on the surface. In equatorial regions, where the Coriolis effect due to the Earth's rotation vanishes, the resulting wind-drift current moves in the same direction as the wind (see [1]). However, in non-equatorial regions the Coriolis effect, arising because of the Earth's spin around its polar axis, is of overriding importance: the wind-driven stress (acting in the direction of the wind) is balanced not only by frictional forces opposing it but also by the Coriolis force. The outcome is a deflection of the surface ocean current from the direction of the wind, to the right in the northern hemisphere and to the left in the southern hemisphere (see [11]).

The deflection of surface currents was first noticed by the Norwegian explorer F. Nansen during the arctic *Fram* expedition (1893–1896). Nansen observed that the ice, rather than moving

in the same direction as the wind, was moving consistently to the right of the wind direction. He discerned that this was due to the effect of the Earth's rotation and reasoned that, as the depth increased, each successive layer of water, moving over the one below it like a wind, would produce an increasing deviation until, at a certain depth, the flow direction would be opposite to that at the surface [8]. Nansen turned to the Swedish physicist V. W. Ekman to provide theoretical support for his observations and reasoning. Ekman's subsequent theory of wind-driven currents stands more than a century after its introduction [7] as the basis for our understanding of wind-driven ocean circulation. While Ekman's theory is also relevant for the air flow in the atmospheric planetary boundary layer (see [3]), our concern will be wind-drift ocean currents. These surface currents regulate the global climate by transporting the heat stored in the upper ocean, thus moderating the extremes of temperature on our planet. The oceans cover over 70% of the Earth's surface and water can absorb and release large amounts of heat without a large increase in temperature. IPCC $5^{\text{th}}$ Assessment Report from 2014 estimates that most of the excess heat trapped by greenhouse gases has been stored within the upper 75 m of the oceans, while the ocean heat content in 2018 was larger than any other year since observations began in the 1950s (see [2]).

Numerous field studies were devoted to verify Ekman's theory. While the predicted deflection of the surface current from the wind direction is observed at mid-latitudes, the deflection angle appears to differ substantially from the of $45^\circ$ value of Ekman's classical theory, being typically much lower (it can be reduced to about $20^\circ$) but larger values (in excess of $50^\circ$) are also encountered. Moreover, the deviation of the surface current from the wind is typically larger during the day than during the night (see [9]). These discrepancies are ascribed to Ekman's oversimplified hypothesis of constant eddy viscosity, a depth-dependent eddy viscosity being typically essential for realistic predictions. Since field data shows that the class of relevant eddy viscosities feature quite different behaviours (the intensity could increase or decrease with depth, but specific regions present non-monotonic types with multiple local extrema) and the available explicit solutions for non-constant eddy viscosity are very scarce (see the discussion in [3]), one has to rely on case-by-case numerical simulations. This type of approach makes it very difficult to identify the important factors that control the size of the deflection angle. We propose an alternative method: by developing a perturbative approach, we provide a generally valid formula that predicts the deviation of the deflection angle from the classical $45^\circ$ reference value. In particular, our approach explains why an eddy viscosity that increases with depth produces deflection angles less than $45^\circ$, while an eddy viscosity that decreases with depth yields deflection angles larger than $45^\circ$.

## 2 Background

For our purposes it is convenient to use a locally valid Cartesian coordinate system with $x$, $y$, and $z$ aligned eastward, northward and upward, respectively, and with the corresponding fluid velocity components denoted by $u$, $v$ and $w$, respectively. In non-equatorial regions, away from surface, bottom and coastal boundary layers the ocean flow is geostrophic (arising from a balance between the pressure gradient force and the Coriolis force), whereas in the mixed layer near the surface (the upper 200-300 m) one has to account for the wind-drift (see [11]). We consider non-equatorial open ocean regions since equatorial flows present peculiar features that are not encountered elsewhere (the vanishing of the meridional component of the Coriolis force at the Equator leads to a breakdown of the geostrophic balance, while its

change of sign across the Equator produces an effective waveguide, with the Equator acting as a fictituous natural boundary that facilitates azimuthal flow propagation – see the discusions in [1, 4]). Since the ratio of vertical speed to horizontal speed is about $10^{-4}$ (see [11]), we neglect the vertical motion and consider an open ocean region with a horizontal geostrophic flow field $(\hat{u},\, \hat{v})$, subjected to a wind stress $(\tau^1,\, \tau^2)$ along its surface. For a homogeneous fluid of density $\rho_0$ the vertical component of the geostrophic flow is zero and the horizontal geostrophic flow depends on the magnitude of the pressure gradient (see [11]):

$$(\hat{u},\, \hat{v}) = \Big( -\frac{1}{f\rho_0}\,\frac{\partial p}{\partial y}\,,\, \frac{1}{f\rho_0}\,\frac{\partial p}{\partial x}\Big)\,, \tag{2.1}$$

where $p$ is the pressure and $f = 2\omega \sin\phi$ is the Coriolis parameter, equal to twice the vertical component of the Earth's rotation vector ($\omega \approx 7.272 \times 10^{-5}\,\mathrm{rad\,s^{-1}}$ and $\phi$ being the radian frequency of Earth's rotation and the latitude, respectively). Neglecting vertical motion means that the pressure distribution is hydrostatic, so that $(\hat{u},\, \hat{v})$ is depth-independent and, assuming steady wind conditions and a turbulent mixing parametrized by a constant vertical eddy viscosity coefficient $K$, the balance between frictional and Coriolis forces can be expressed in the form of the following differential equations for the latitudinal and longitudinal velocity components of the wind drift, as a function of depth:

$$\begin{cases} -f\,(v-\bar{v}) \;=\; K\,\dfrac{\partial^2 u}{\partial z^2}\,, \\[2ex] f\,(u-\bar{u}) \;=\; K\,\dfrac{\partial^2 v}{\partial z^2}\,. \end{cases} \tag{2.2}$$

The wind stress at the surface $z = 0$ is given by

$$(\tau^1,\, \tau^2) = \rho_0 K \Big(\frac{\partial u}{\partial z}\,,\, \frac{\partial v}{\partial z}\Big)\,, \tag{2.3}$$

and the boundary condition

$$(u-\bar{u},\, v-\bar{v}) \to (0,0) \quad \text{as} \quad z \to -\infty\,, \tag{2.4}$$

expresses the fact that the wind-drift current is insignificant at great depths. Ekman's solution to this problem is, in complex variables notation,

$$(u-\bar{u}) + \mathrm{i}(v-\bar{v}) = \frac{\sqrt{2}}{\rho_0 f d}\;[\tau_1 + \mathrm{i}\tau_2]\,\exp\Big(\frac{z}{d}\Big)\,\exp\Big\{\mathrm{i}\Big(\frac{z}{d} - \frac{\pi}{4}\Big)\Big\}\,, \tag{2.5}$$

where $d = \sqrt{2K/f}$ is the Ekman-layer reference depth, with $\pi d$ representing the lower boundary of the Ekman layer – the near-surface region of the ocean affected by the movement of wind and frictional influence, typically about 30–200 m deep. The wind-driven horizontal flow component (2.5) is independent of the geostrophic flow field $(\hat{u},\, \hat{v})$, with the surface current directed 45° to the right/left of the surface wind stress in the northern/southern hemisphere, with velocities decaying and rotating with depth to the right/left to form a spiral (see Fig. 1).

Observational evidence for Ekman's solution (2.5) is provided by the wind-driven currents in the Southern Ocean (see [13]). However, most field studies of wind-drift ocean currents report systematic differences (see e.g. [6]). Ekman's basic predictions, that the wind-drift current surface veers at the surface to the right/left of the wind (in the northern/southern hemisphere) and that with increasing depth the current speed is reduced, while the direction

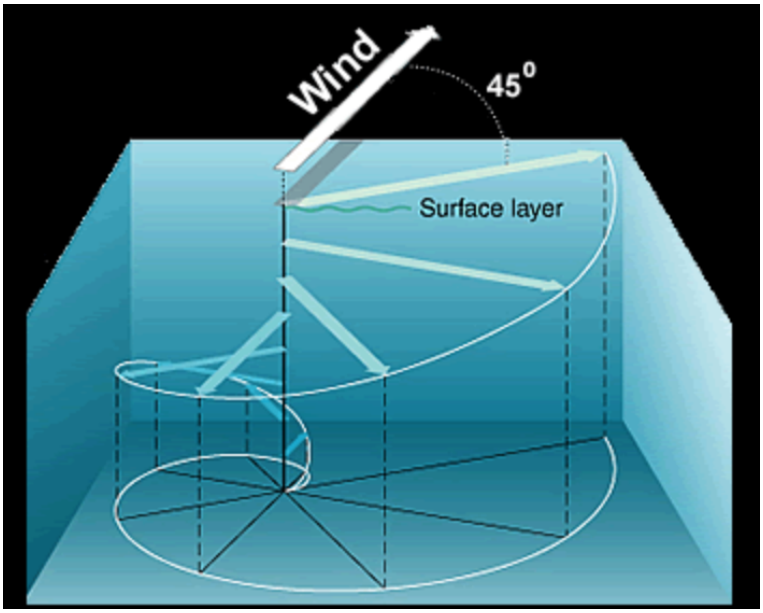


Figure 1: Sketch of the structure of wind-driven currents at mid-latitudes: the vertical motion is very weak and, according to Ekman theory, the horizontal current velocity vectors form a descending spiral from an angle of 45° (to the right/left direction of the wind in the northern/southern hemisphere) at the water surface to an angle of 180° (opposite to the wind direction), at a Ekman-layer depth. The vectors rapidly decrease in length (speed) as the depth increases, being reduced by a factor of $e^{\pi} \approx 23$ at the bottom of the Ekman layer (Image credit: NOAA).

rotates farther away from the wind direction following a spiral, are generally accepted but the details are generally not. It is by now recognized that the assumption of constant eddy viscosity is an extreme simplification and a depth-dependent eddy viscosity $K(z)$ is necessary, so that instead of (2.2) we have the system

$$\begin{cases} -f\,(v-\bar{v}) = \dfrac{\partial}{\partial z}\left(K(z)\,\dfrac{\partial u}{\partial z}\right), \\ f\,(u-\bar{u}) = \dfrac{\partial}{\partial z}\left(K(z)\,\dfrac{\partial v}{\partial z}\right), \end{cases} \tag{2.6}$$

with the boundary conditions (2.3) and (2.4); see [5]. We regard the physically relevant eddy viscosities $K(z)$ as perturbations of the asymptotic reference value $K_0 = \lim_{z\to-\infty} K(z) > 0$, so that

$$K(z) \;=\; K_0 + \varepsilon K_1(z)\,, \qquad z \le 0\,, \tag{2.7}$$

where $\varepsilon \ll 1$ and the asymptotic rate of convergence is faster than quadratic, that is, there exist constants $a$, $b$, $c > 0$ such that

$$|K_1(z)| \le \frac{a}{1+b|z|^{2+c}}\,, \qquad z \le 0\,.$$

Field data shows that quite often the perturbation $K_1$ actually converges exponentially fast to zero at great depths (see the discussion in [3]).

## 3 Methods

To simplify notation, we use the complex function

$$\Psi \;=\; U + iV\,, \qquad \text{with} \quad U = u - \bar{u}\,, \quad V = v - \bar{v}\,,$$

and perform the variable change

$$s \;=\; s(z) \;\doteq\; K_0 \int_z^0 \frac{-1}{K(y)}\, dy, \tag{3.8}$$

to write the system (2.6) more compactly as the complex-valued second order differential equation

$$\Psi''(s) \;=\; \mathrm{i}\kappa(s)\Psi(s) \qquad\qquad s < 0\,, \tag{3.9}$$

where

$$\kappa(s) \;= \frac{f}{K_0^2}\, K(z) \qquad\qquad s \le 0\,. \tag{3.10}$$

The boundary conditions (2.3) and (2.4) are transformed to

$$\Psi'(0) \;=\; \frac{1}{\rho_0 K_0}\,(\tau^1 + \mathrm{i}\tau^2) \qquad \text{and} \qquad \Psi \;\to\; 0 \quad \text{as} \quad s \to -\infty\,, \tag{3.11}$$

respectively. Writing

$$\kappa(s) \;=\; \frac{f}{K_0} + \varepsilon k(s)\,, \qquad s \le 0\,, \tag{3.12}$$

we set

$$\Psi(s) \;=\; \Psi_0(s) + \varepsilon\psi(s) + o(\varepsilon)\,, \qquad s \le 0\,, \tag{3.13}$$

where $\Psi_0$ is the explicit classical Ekman solution

$$\Psi_0(s) \;=\; \frac{1-\mathrm{i}}{\rho_0\sqrt{2fK_0}}(\tau^1 + i\tau^2)\,\mathrm{e}^{(1+\mathrm{i})\lambda s} \qquad \text{with} \quad \lambda \;=\; \sqrt{f/(2K_0)}\,. \tag{3.14}$$

Inserting (3.13) in (3.9) one obtains

$$\Psi_0''(s) + \varepsilon\psi''(s) \;=\; \mathrm{i}\Big(\frac{f}{K_0} + \varepsilon k(s)\Big)\Big(\Psi_0(s) + \varepsilon\psi(s)\Big) + o(\varepsilon).$$

Dividing by $\varepsilon$ and letting $\varepsilon \to 0$, this yields a linear, non-homogeneous second order differential equation for the perturbation $\psi$, namely

$$\psi''(s) - \mathrm{i}\,\frac{f}{K_0}\,\psi(s) \;=\; \mathrm{i}k(s)\Psi_0(s)\,, \tag{3.15}$$

to be solved with homogeneous boundary and asymptotic conditions:

$$\psi'(0) \;=\; 0, \qquad\qquad \psi \;\to\; 0 \quad \text{as} \quad s \to -\infty. \tag{3.16}$$

The solution to (3.15)-(3.16) can be expressed as the convolution

$$\psi(s) \;=\; \mathrm{i}\int_{-\infty}^0 G(s,t)\,k(t)\Psi_0(t)\,\mathrm{d}t\,, \qquad s \le 0\,, \tag{3.17}$$

where for $t<0$ the Green's function $w(s)=G(s,t)$ provides a solution to

$$\left\{\begin{array}{lll} w''(s)-\mathrm{i}\,\frac{f}{K_0}\,w(s) \;=\; 0, & s\in(-\infty,t)\cup(t,0)\,, & \\ w'(0)\;=\;0, & w'(t-)-w'(t+)\;=\;1, & w(s)\to 0 \quad \text{as } s\to-\infty. \end{array}\right. \tag{3.18}$$

The solution to (3.18) is of the form

$$w(s) \;=\; \left\{\begin{array}{ll} A\Big[\mathrm{e}^{(1+\mathrm{i})\lambda s}+\mathrm{e}^{-(1+\mathrm{i})\lambda s}\Big] & \text{for } s\in(t,0)\,, \\ B\mathrm{e}^{(1+i)\lambda s} & \text{for } s\in(-\infty,t)\,. \end{array}\right. \tag{3.19}$$

Using the continuity of $w$ and the jump condition in the derivative at $s=t$, we find

$$A \;=\; \frac{1-\mathrm{i}}{4\lambda}\,\mathrm{e}^{(1+\mathrm{i})\lambda t}\,, \qquad B \;=\; \frac{1-\mathrm{i}}{4\lambda}\Big[\mathrm{e}^{(1+\mathrm{i})\lambda t}+\mathrm{e}^{-(1+\mathrm{i})\lambda t}\Big]\,,$$

so that the solution to (3.15)-(3.16) is given by

$$\begin{aligned} \psi(s) \;&=\; \frac{1}{2\rho_0 f}\,(\tau^1+i\tau^2)\int_s^0\Big[\mathrm{e}^{(1+i)\lambda t}+\mathrm{e}^{-(1+i)\lambda t}\Big]\mathrm{e}^{(1+i)\lambda(s+t)}k(t)\,\mathrm{d}t \\ &\quad+\frac{1}{2\rho_0 f}\,(\tau^1+i\tau^2)\int_{-\infty}^s \mathrm{e}^{2(1+i)\lambda t}\Big[\mathrm{e}^{(1+i)\lambda s}+\mathrm{e}^{-(1+i)\lambda s}\Big]k(t)\,\mathrm{d}t\,. \end{aligned} \tag{3.20}$$

At $s=0$ one finds

$$\psi(0) \;=\; \frac{1}{\rho_0 f}\,(\tau^1+i\tau^2)\int_{-\infty}^0 \mathrm{e}^{2(1+i)\lambda t}k(t)\,\mathrm{d}t\;\;,$$

so that (3.14) yields

$$\Psi(0) \;=\; \frac{1}{\rho_0\sqrt{fK_0}}\,(\tau^1+i\tau^2)\,\mathrm{e}^{-i\pi/4}\Big\{1+\varepsilon\,\frac{1+i}{2\lambda\sqrt{2}}\int_{-\infty}^0 \mathrm{e}^{2(1+i)\lambda t}k(t)\,\mathrm{d}t\Big\}\;. \tag{3.21}$$

The formula

$$\frac{\mathrm{d}}{\mathrm{d}\varepsilon}\arg(1+\varepsilon\xi)\Big|_{\varepsilon=0}=\mathrm{Im}(\xi)\,,\qquad \xi\in\mathbb{C}\,,$$

enables us to express the change of the deflection angle due to the perturbation as

$$\mathrm{Im}\Big\{\frac{1+i}{2\lambda\sqrt{2}}\int_{-\infty}^0 \mathrm{e}^{2(1+i)\lambda t}k(t)\,\mathrm{d}t\Big\}=\frac{1}{2\lambda}\int_{-\infty}^0 \mathrm{e}^{2\lambda t}k(t)\sin\big(2\lambda t+\tfrac{\pi}{4}\big)\,\mathrm{d}t\,. \tag{3.22}$$

A positive/negative value of the integral $\int_{-\infty}^0 \mathrm{e}^{2\lambda t}k(t)\sin\big(2\lambda t+\frac{\pi}{4}\big)\,\mathrm{d}t$ corresponds to an increase/decrease of the deflection angle from the reference value $\pi/4$.

# 4 Discussion

The formula (3.22) for the change of the deflection angle due to the perturbation provides insight into the way the depth-variation of the eddy viscosity influences the deflection angle. Note that the change of variables (3.8) preserves the monotonicity properties, and that, as $s$ decreases from 0 towards $-\infty$, the function $\mathrm{e}^{2\lambda t}k(t)\sin\big(2\lambda t+\frac{\pi}{4}\big)$ changes sign alternatly,

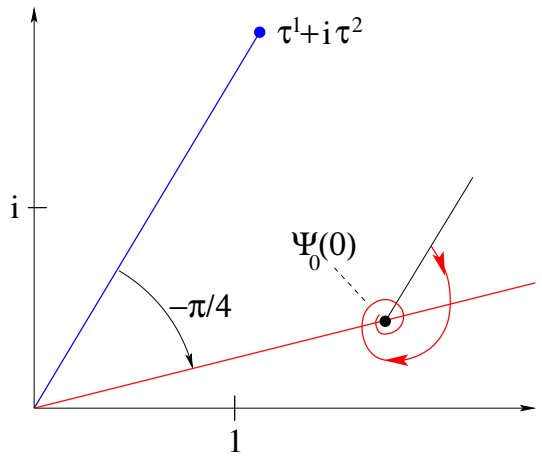


Figure 2: The center of the spiral is on the ray deflected by an angle of $\pi/4$ from the direction of the steady wind. The perturbation $K_0 + \varepsilon k(t)$ of the constant eddy viscosity $K_0$ produces a shift in different directions, depending on the sign of the integral in (3.22).

being positive for $s \in I_0 := (-\frac{\pi}{8\lambda}, 0)$, negative on $I_j^- := (-\frac{(5+8j)\pi}{8\lambda}, -\frac{(1+8j)\pi}{8\lambda})$ and positive on $I_j^+ := (-\frac{(9+8j)\pi}{8\lambda}, -\frac{(5+8j)\pi}{8\lambda})$ for integers $j \geq 0$. Moreover, since its antiderivative is $\frac{1}{2\sqrt{2}}\, \mathrm{e}^{2\lambda t} k(t) \sin(2\lambda t)$, we have

$$\int_{-\infty}^{0} \mathrm{e}^{2\lambda t} \sin\left(2\lambda t + \tfrac{\pi}{4}\right) \mathrm{d}t \;=\; 0\,, \qquad \int_{I_0} \mathrm{e}^{2\lambda t} \sin\left(2\lambda t + \tfrac{\pi}{4}\right) \mathrm{d}t \;=\; \tfrac{1}{2\sqrt{2}}\, \mathrm{e}^{-\frac{\pi}{4}}\,,$$

with

$$\int_{I_0} \mathrm{e}^{2\lambda t} \sin\left(2\lambda t + \tfrac{\pi}{4}\right) \mathrm{d}t \;=\; \frac{\mathrm{e}^{-\frac{\pi}{4}}}{4}\,, \qquad \int_{I_j^-} \mathrm{e}^{2\lambda t} \sin\left(2\lambda t + \tfrac{\pi}{4}\right) \mathrm{d}t \;=\; -\,\frac{\mathrm{e}^{-2\pi j}\left(\mathrm{e}^{-\frac{\pi}{4}} + \mathrm{e}^{-\frac{5\pi}{4}}\right)}{4}\,,$$

$$\int_{I_j^+} \mathrm{e}^{2\lambda t} \sin\left(2\lambda t + \tfrac{\pi}{4}\right) \mathrm{d}t = \frac{\mathrm{e}^{-2\pi j}\left(\mathrm{e}^{-\frac{5\pi}{4}} + \mathrm{e}^{-\frac{9\pi}{4}}\right)}{4}\,,$$

for $j \geq 0$. The sequence $\{d_j\}_{j\geq 0}$ of the absolute values of these integrals converges exponentially fast to zero and is strictly decreasing starting with $j \geq 1$ but $d_2 \approx 0.005 < d_0 \approx 0.114 < d_1 \approx 0.118$. Testing the case when the perturbation $k$ is constant on each of the intervals $I_j^{\pm}$ shows that a decreasing eddy viscosity does not necessarily yield $\int_{-\infty}^{0} \mathrm{e}^{2\lambda t} k(t) \sin\left(2\lambda t + \frac{\pi}{4}\right) \mathrm{d}t > 0$, the key factor being the relative size of the values assigned to the intervals $I_0$ and $I_0^-$. Note that $I_0$ corresponds to the upper eighth part of the Ekman layer of depth $d = \frac{\pi}{\lambda}$, while $I_0^-$ extends within the lower half of the Ekman layer. This analysis shows that an eddy viscosity that increases/decreases with depth in the Ekman layer does not always induce a deflection angle that lags/exceeds $\pi/4$, even if this implication holds for Madsen's model of a linear increase with depth [10] (which then motivated the expectation that this is a universally valid feature – see the discussion in [9]). Moreover, if the eddy viscosity at the top of the Ekman layer (within $I_0$) is lower than towards the middle of the layer, then the negative contribution from $I_0^-$ dominates the positive one from $I_0$, with a negative integral as the typical outcome. This explains why in arctic regions the deflection angle is below $\pi/4$, since the ice cover tends to quell the turbulence near the ocean surface.

With regard to the observed day-night changes in the deflection angle, note that solar heating quenches turbulence throughout the Ekman layer during the day, while turbulence becomes stronger at night due to nocturnal convection, as the vertical extent of the Ekman layer (typically less than 100 m) coincides with the depth above which the downward flux of solar energy exceeds 1 % of that entering at the sea surface (see [15]). The nocturnal increase of the eddy viscosity occurs across the upper half of the Ekman layer (the change in the lower half being rather insignificant). This amplifies the contribution from the region $I_0^-$, leading thus typically to an overall negative integral in (3.22) with the result that the deflection angle is smaller during the night.

## References


[1] Boyd, J. P. (2018). *Dynamics of the equatorial ocean*. Springer.

[2] Cheng, L., Abraham, J., Hausfather, Z., and Trenberth, K. E. (2019). How fast are the oceans warming? *Science* 363, 128–129.

[3] Constantin, A., and Johnson, R. S. (2019). Atmospheric Ekman flows with variable eddy viscosity. *Boundary-Layer Meteorology* 170, 395–414.

[4] Constantin, A., and Johnson, R. S. (2019). Ekman-type solutions for shallow-water flows on a rotating sphere: A new perspective on a classical problem. *Physics of Fluids* 31, 021401.

[5] Cronin, M. F., and Kessler, W. S. (2009). Near-surface shear flow in the tropical Pacific Cold Tongue Front. *J. Phys. Oceanogr.* 39, 1200–1215.

[6] Cronin, M. F., and Tozuka, T. (2016). Steady state ocean response to wind forcing in extratropical frontal regions. *Scientific Reports (Nature)* 6, 28842.

[7] Ekman, V. W. (1905). On the influence of the Earth's rotation on ocean-currents. *Ark. Mat. Astron. Fys.* 2, 1–52.

[8] Huntford, R. (2002). *Nansen: The Explorer as Hero*. Abacus.

[9] Krauss, W. (1993). Ekman drift in homogeneous water. *J. Geophys. Res.* 98, 187–209.

[10] Madsen, O. S. (1977). A realistic model of the wind-induced Ekman boundary layer. *J. Phys. Oceanogr.* 7, 248–255.

[11] Marshall, J., and Plumb, R. A. (2016). *Atmosphere, ocean and climate dynamics: an introductory text*. Academic Press.

[12] Polton, J. A., Lenn, Y.-D., Elipot, S., Chereskin, T. K. and Sprintall, J. (2013). Can Drake Passage observations match Ekman's classic theory? *J. Phys. Oceanogr.* 43, 1733–1740.

[13] Roach, C. J., Phillips, H. E., Bindoff, N. L., and Rintoul, S. R. (2015). Detecting and characterizing Ekman currents in the Southern Ocean. *J. Phys. Oceanogr.* 45, 1205–1223.

[14] Stacey, M. W., Pond, S., and Leblond, P.H. (1986). A wind-forced Ekman spiral as a good statistical fit to low-frequency currents in a coastal strait. *Science* 233, 470–472.

[15] Woods, J. (2002). Laminar flow in the ocean Ekman layer. *Meteorology at the Millenium* (Ed. R. P. Pearce), pp. 220–232, Elsevier.